High-throughput identification of RNA nuclear enrichment sequences

Chinmay J Shukla[1,2,3,4], Alexandra L McCorkindale[1,7], Chiara Gerhardinger[1,2], Keegan D Korthauer[3,5], Moran N Cabili[2], David M Shechner[1,2], Rafael A Irizarry[3,5], Philipp G Maass[1*], John L Rinn[1,2,6*]

1. Department of Stem Cell and Regenerative Biology, Harvard University, Cambridge, Massachusetts 02138, USA

2. Broad Institute of MIT and Harvard, Cambridge, Massachusetts 02139, USA

3. Department of Biostatistics and Computational Biology, Dana-Farber Cancer Institute, Cambridge, Massachusetts 02115, USA

4. Program in Biological and Biomedical Sciences, Harvard Medical School, Boston, Massachusetts 02115, USA

5. Department of Biostatistics, Harvard T.H. Chan School of Public Health, Boston, Massachusetts 02115, USA

6. Department of Pathology, Beth Israel Deaconess Medical Center, Boston, Massachusetts 02215, USA

7. Berlin Institute for Medical Systems Biology, Max Delbrück Center for Molecular Medicine, Berlin-Buch 13125, Germany

* - These authors contributed equally

Author contact information: J.L.R. - johnrinn@fas.harvard.edu

Summary

One of the biggest surprises since the sequencing of the human genome has been the discovery of thousands of long noncoding RNAs (lncRNAs)[1–6]. Although lncRNAs and mRNAs are similar in many ways, they differ with lncRNAs being more nuclear-enriched and in several cases exclusively nuclear[7,8]. Yet, the RNA-based sequences that determine nuclear localization remain poorly understood[9–11]. Towards the goal of systematically dissecting the lncRNA sequences that impart nuclear localization, we developed a massively parallel reporter assay (MPRA). Unlike previous MPRAs[12–15] that determine motifs important for transcriptional regulation, we have modified this approach to identify sequences sufficient for RNA nuclear enrichment for 38 human lncRNAs. Using this approach, we identified 109 unique, conserved nuclear enrichment regions, originating from 29 distinct lncRNAs. We also discovered two shorter motifs within our nuclear enrichment regions. We further validated the sufficiency of several regions to impart nuclear localization by single molecule RNA fluorescence *in situ* hybridization (smRNA-FISH). Taken together, these results provide a first systematic insight into the sequence elements responsible for the nuclear enrichment of lncRNA molecules.

Main

RNA subcellular localization provides a fundamental mechanism through which cells modulate and utilize the functions encoded in their transcriptomes[16]. This spatial layer of gene regulation is known to be critical in a variety of contexts, including asymmetric cell divisions[17], embryonic development[18–20], and signal transduction[21]. Previous work has identified a small number of *cis*-acting mRNA localization elements, using genetic approaches or hybrid reporter constructs to decipher sequences required for localization to different parts of the cell[16,18]. These elements are

51 often located in 3´ untranslated regions (UTRs), and range from five to several hundred
52 nucleotides in length[9–11,18]. Yet, the sequences and structures responsible for RNA localization
53 remain inchoate. In contrast to mRNAs that are mostly localized outside the nucleus, lncRNAs
54 are enriched or retained in the nucleus. Increasing evidence suggests that many lncRNAs may
55 reside in the nucleus for the purpose of regulating nuclear processes, including formation of
56 paraspeckles, topological organization of the nucleus, and regulation of gene expression[1,3,4,22].
57 However, while it is now evident that lncRNAs have important functions in the nucleus[22], very little
58 is known about specific sequence elements driving their nuclear enrichment[9–11].
59
60 To elucidate which sequences drive lncRNA nuclear enrichment, we developed a high-throughput
61 approach for identifying nuclear enrichment elements. Our approach, derived from a massively
62 parallel reporter assay (MPRA)[12–15, 23], is based on a previous assay demonstrating that the native
63 cytosolic localization of a noncoding RNA reporter (a frame-shifted *Sox2* mutant, "fsSox2") can
64 be altered by appending this reporter with additional RNA sequences[9]. The MPRA we designed
65 highly parallelizes this assay by appending thousands of oligos to fsSox2. Briefly, we selected 38
66 lncRNAs with diverse subcellular localization patterns: from single nuclear foci (*e.g. XIST, ANRIL,*
67 *ANCR, PVT1, KCNQ1OT1, FIRRE*) to broadly diffuse cytosolic patterns (*e.g.* NR_024412,
68 XLOC_012599)[24]. We generated a pool of 11,969 oligos 153 nucleotides in length, each with a
69 unique barcode, that tiles each of the 38 lncRNAs. This pool was expressed in HeLa cells followed
70 by nuclear isolation and targeted deep sequencing to determine the partitioning of each fsSox2
71 variant (**Figure 1A, Extended Data Table 1**, *Methods*). All experiments were performed as six-
72 biological replicates to ensure sufficient statistical power for our analytical model, and accurately
73 estimate in-group variance (*see below, Methods*).
74

To identify lncRNA nuclear enriched regions we implemented a statistical method that merges individual nucleotides into longer aggregate regions[25]. We further ranked candidate regions using a newly defined summary statistic, that generates a null distribution for this statistics by permuting sample labels, and uses this null distribution to assigns *p*-values (**Extended Data Figure 1;** *Methods*). Our approach leverages the inter-replicate variability inherent in high throughput reporter assays and allows us to sensitively and accurately discover nuclear enriched RNA segments which we term "differential regions" (DRs). Importantly, our method allows us to identify DRs greater than individual oligos based on their coherence across larger regions.

To test the performance of our assay and analytic method we first focused on a well established nuclear lncRNA *MALAT1.* Previous work demonstrated that two elements termed Region E and Region M, derived from the lncRNA *MALAT1,* are particularly potent RNA nuclear localization signals[11]. We examined the nuclear enrichment of all fsSox2 pool variants bearing elements derived from lncRNA *MALAT1* (*Methods*). Consistent with the previous study, nucleotides derived from Region E and Region M were highly enriched in the nucleus compared to those residing elsewhere in the human *MALAT1* lncRNA. Thus, our assay can recapitulate known RNA localization signals and our analysis approach can identify localization domains longer than a given tiled oligos.

Next we sough to agnostically and systematically investigate nuclear enrichment regions harbored within 38 lncRNAs. Our analysis identified 109 DRs (FDR < 0.1) originating from 29 distinct lncRNAs that were significantly enriched in nuclear fractions, relative to whole cell lysates (**Extended Data Table 2**). Two of these DRs overlap and subsume Region M while another DR overlaps with Region E within the *MALAT1* lncRNA (**Figure 1B, 1C**). To confirm that our approach was robust, we compared the significant DRs to all other regions represented in our pool and

found them significantly more nuclear enriched (**Figure 1D**; $P < 1/10^6$, Mann-Whitney Test; *Methods*). The localization patterns of the selected 38 lncRNAs have been previously parsed into five smRNA-FISH classes[24]. These included lncRNAs strictly nuclear (FISH Class I), those that are diffusely localized in the cytoplasm (FISH Class V), and three intermediate classes (FISH Classes II–IV). Our MPRA approach discovered DRs derived from lncRNAs in all five FISH classes (**Figure 2A–E**). Notably, the number of DRs within each class broadly correlated with the degree of nuclear localization observed by smRNA-FISH (**Figure 2F**). Many strictly-nuclear lncRNAs (FISH Class I) harbor multiple DRs, possibly indicating the presence of a redundant nuclear localization motif. For example, we discovered 18 DRs in *XIST* and 10 DRs in *MALAT1* and some of the DRs we discovered in *XIST* overlap with previously-described repeat elements – RepC and RepD.

We further analyzed the evolutionary conservation, length distribution, and sequence content of these putative nuclear localization sequences. We used phastCons[26,27] scores to assess evolutionary conservation, and we observed significantly higher scores among our DRs than in other lncRNA regions tiled by our MPRA (**Figure 2G**; $P < 1/10^6$, Mann-Whitney Test; *Methods*). The lengths of our DRs ranged from 80–740 nucleotides (nt), with an average of 300 nt (**Extended Data Figure 6A**). While we detected a weak correlation between the length of a given lncRNA and number of DRs within (**Extended Data Figure 6B**), this analysis is confounded by inconsistent length of lncRNAs across the five FISH classes. Finally, we did not observe a difference in GC content between the DRs and other sequences in our tiled lncRNAs (**Extended Data Figure 6C**).

We hypothesized that our DRs might harbor common sequence motifs or protein-binding preferences. To test this, we searched for motifs that were more prevalent among the DRs than

in other regions of the lncRNAs, using the MEME software package[28]. We identified a 57 nt motif occuring 18 times exclusively in *XIST*, and not elsewhere in the human genome (**Figure 3A–C**). Another, 15 nt "C-rich" motif was found in 52 DRs of 21 different lncRNAs (**Figure 3D–F**), and we discovered four additional motifs closely related to the described here (**Extended Data Figure 7A–D**). Similarly, k-mer analysis[29] revealed several C-rich 4-mers that were mildly predictive of a DR (**Extended Data Figure 7E**). In total, we discovered six motifs and confirmed that the nucleotides overlapping these motifs were significantly enriched in the nucleus ($P < 1/10^6$, Mann-Whitney Test, *Methods*), compared to all other regions tiled in our MPRA (**Figure 3G**). Since the C-rich motif occured in more than 50 distinct DRs of diverse lncRNAs, we postulated that this motif could function as a global RNA nuclear localization element. To test this, we examined the nuclear–cytoplasmic localizations of all human transcripts containing this motif, using fractionation RNA-Seq data from ENCODE[30]. We observed a modest increase ($P < 1/10^6$, Mann-Whitney Test) in nuclear localization of transcripts with the C-rich motifs across all 11 ENCODE TIER 2 cell lines (**Figure 3H, I, Extended Data Figure 8**). This further demonstrates the potential power of our MPRA to discover functional elements that may be missed by classic RNA localization studies. A similar C-rich motif was recently discovered by another group and has been investigated in mechanistic detail (Igor Ulitsky – personal communication).

We independently tested if these motifs are sufficient for nuclear localization using smRNA-FISH. Briefly, we appended the consensus motif sequences identified by our MPRA to the 3' end of the cytosolic fsSox2 reporter and electroporated these constructs in HeLa cells [9]. We then performed smRNA-FISH[31] and did a double blinded quantification of the signals in more than 300 nuclei for each electroporated construct using StarSearch[31] (*Methods*). We observed that ~30 % of *fsSox2* transcripts localized in the nucleus but appending the repetitive *XIST* motif (Motif 1) slightly increased nuclear localization to ~40% (**Figure 4**; $P = 0.03$, Mann-Whitney Test). Appending the

C-rich motif (Motif 2) did not significantly affect the localization of *fsSox2* (**Figure 4**). These results suggest that small motifs could exhibit a weak effect of RNA nuclear enrichment, but are insufficient for localization.

Since we observed only a small effect for a short motif like the *XIST* motif to affect nuclear enrichment, we next asked next whether longer regions identified by our MPRA would show a stronger effect. To this end we generated multiple *fsSox2*:DR constructs (DRs: *MALAT1, TUG1, XIST*) and compared their subcellular localization to the native *fsSox2* transcript by smRNA-FISH. We found that *MALAT1* "Region M" significantly increased nuclear enrichment of *fsSox2* (**Figure 4**; $P < 1/10^6$, Mann-Whitney Test). Similarly, a novel *TUG1* DR identified by our MPRA, as well as *the XIST* DR, which harbors the *XIST* motif, showed also nuclear enrichment of fsSox2 (**Figure 4**; $P < 1/10^6$, Mann-Whitney Test; *Methods*). Thus, the longer DRs identified in our MPRA are sufficient to significantly change the nuclear enrichment of a cytosolic transcript where as shorter motifs could not.

Collectively, our study has several implications. First, we have demonstrated a new functional MPRA which can identify longer nuclear enrichment sequences by computationally stitching short (110 bp) oligonucleotides together. Second, we have discovered motifs common to many DRs that tend to be nuclear enriched. However, these small motifs exhibit only a mild propensity for nuclear enrichment when tested independently. Conversely, longer DRs were sufficient to change the nuclear enrichment of a cytosolic reporter. While this manuscript was in preparation, a C-rich motif similar to that identified by our MPRA was also found by other investigators and functionally tested by mutation and protein binding preferences (Igor Ulitsky – personal communication). Third, many DRs identified in our study did not harbor any motif and many lncRNAs harbored multiple DRs.

Taken together, these results indicate that there does not appear to be a small universal sequence motif that is sufficient for nuclear enrichment. Rather, we propose that multiple unique sequences co-occurring within a longer structured region are responsible for nuclear enrichment for each lncRNA. While additional studies will need to confirm this prediction, our study provides an important initial map and a systematic, unbiased framework to explore RNA nuclear enrichment signals.

Methods

Oligo Pool Design

We designed 153-mer oligonucleotides to contain, in order, the 16-nt universal primer site ACTGGCCGCTTCACTG, a 110-nt variable sequence, a 10-nt unique barcode sequence and the 17-nt universal primer site AGATCGGAAGAGCGTCG. The unique barcodes were designed as described previously while the variable sequences were obtained by tiling lncRNA sequences. The resulting oligonucleotide libraries were synthesized by Broad Technology Labs.

ePCR amplification of oligopool

The synthesized oligopool was amplified by emulsion-PCR (ePCR, Micellula DNA Emulsion & Purification Kit, Chimerx), according to the manufacturers' instructions. The e-PCR primers where designed to add the Age I / Not I restriction sites to the synthesized oligos for subsequent cloning (Age I primer: AATAATACCGGTACTGGCCGCTTCACTG; Not I primer: GAGGCCGCG GCCGCCGACGCTCTTCCGATCT). To determine the oligos representation of the ePCR amplified oligo pool (based on the unique 3' barcode of each oligo), 1 ng of the amplified oligo pool was used as input for library preparation (see below) and sequenced on a MiSeq (SR, Illumina).

200

201 **Cloning**

202 A minCMV promoter (5'-TAGGCGTGTACGGTGGGAGGCCTATATAAGCAGAGCTCGTTTAGT
203 GAACCGTCAGATCGC-3') was cloned upstream of fsSox2[9]. The ePCR-amplified oligopool and
204 the identified motifs and candidate regions were digested with Age I / Not I and inserted 3' of
205 fsSox2. For MPRA-cloning, the ligation reaction (100 ng backbone + 4 x molar excess of
206 oligopool) was transformed into 10 x DH5α tubes (ThermoScientific). A total of 20 ampicillin LB
207 plates were inoculated with the 10 transformation reactions and incubated overnight at 37°C. All
208 bacterial colonies were then scraped in 5 ml of LB per plate and pooled, and the plasmids were
209 purified with the endotoxin-free Qiagen Plasmid Plus Maxi kit (Qiagen). The cloned oligopool was
210 then sequenced on the MiSeq to determine the oligo representation as described above.

211

212 **Cell fractionation**

213 HeLa nuclear and cytoplasmic fractions were isolated as previously described[9]. The success of
214 the fractionations (**Extended Data Figure 2B**) was confirmed by qRT-PCR of the nuclear ncRNA
215 NEAT1 and the cytoplasmic ncRNA SNHG5 in RNA isolated (see below) from whole cells, the
216 pelleted nuclei, and from the cytoplasmic fractions.

217

218 **RNA extraction and qRT-PCR**

219 RNA was isolated by TRIzol (ThermoScientific) - chloroform extraction, followed by isopropanol
220 precipitation, according to standard procedures. 2 μg of BioAnalyzer-validated RNA were
221 digested with recombinant DNase-I (2.77 U/μl, Worthington #LS006353) at 37°C for 30 min,
222 followed by heat-inactivation at 75°C for 10 min. Reverse transcription was performed with
223 SuperScript III cDNA synthesis kit (ThermoScientific). Quantitative RT-PCR was performed using
224 the FastStart Universal SYBR Green Master mix (Roche) on an ABI 7900. Primers were: NEAT1

forward TGATGCCACAACGCAGATTG, reverse GCAAACAGGTGGGTAGGTGA, and SNHG5 forward GTGGACGAGTAGCCAGTGAA, reverse GCCTCTATCAATGGGCAGACA. After processing the raw data by qPCR Miner[32], the efficiency of each primer set was used to calculate the relative initial concentration of each gene. The relative expression in the nuclear and cytoplasmic fractions was then calculated by normalization to that in the whole cell.

Library preparation

Sequencing libraries were prepared by PCR amplification using PfuUltra II Fusion DNA polymerase (Agilent #600672) and primers designed to anneal to the universal primer site flanking the oligos and to add sequencing index barcode for multiplexing: forward caagcagaagacggcatacgagatCGTGATgtgactggagttcagacgtgtgctcttccgatctACTGGCCGCTTCACTG, reverse AATGATACGGCGACCACCGAGATCTACACTCTTTCCCTACACGACGCTCTTCCGATCT (capital letters indicate (1) the index for the library and (2) the region complementary to the universal primer site). PCR amplification (initial denaturation 95°C – 2 min; cycling 95°C – 30 secs, 55°C – 30 secs, 72°C – 30 sec; final extension 72°C – 10 min) was carried out for 30 cycles followed by triple 0.6x, 1.6x, and 1x SPRI beads (Agencourt AMPure XP, Beckman Coulter) cleanup. The quality and molarity of the libraries was evaluated by BioAnalyzer and the samples were sequenced in a pool of 6 on the Illumina HiSeq2500, full flow cell, single-read 100 bp. To ensure the transfection was successful, we required that at least 70% of the oligo pool was represented back (i.e. had a count of at least one) in the sequencing sample. (**Extended Data Figure 2, 3 and 4**)

Analyzing MPRA Data

Read Mapping and Obtaining Counts Table

To find a unique mapping location for the read, we ensured an exact match between the first 10 read nucleotides and a unique oligo barcode. To ensure that the correct oligo was identified using this barcode match, we allowed only 2 mismatches between the remaining 65 nts of the read sequence and the upstream oligo sequence corresponding to the unique barcode (**Extended Data Figure 1A**). The resulting counts for each oligo in every sample (6 Nuclei and 6 Total) were compiled in a counts table (**Extended Data Figure 1A**).

Normalizing the counts table

The counts table was normalized using a library size correction in order to facilitate comparing counts across samples with different sequencing depths. The library size was calculated as the total number of reads in each sample.

Modeling Nucleotide Counts from Oligo Counts

The counts of a particular nucleotide were modeled by taking the median of counts for every oligo tiling the nucleotide (**Extended Data Figure 1B**). We tried other methods to model nucleotide such as taking the sum of the counts of all oligos tiling the given nucleotide and a probabilistic graphical model as used recently[15] but the simple and intuitive median approach yielded comparable results. Since the offset between subsequent oligos was usually 10 nucleotides, we obtained nucleotide counts also at a 10 nucleotide resolution. The resulting modeled nucleotide counts table (**Extended Data Table 2**) was used to infer differential regions.

Inferring Differential Regions from Modeled Nucleotide Counts

There are 2 main steps in inferring differential regions from modeled nucleotide counts – (i). Identifying potential candidate regions and (ii). Assigning a p-value for each potential candidate region (**Extended Data Figure 1C**). We identified potential candidate regions by calculating the

median of the difference between nuclear counts and total counts across all 6 replicates at each nucleotide and then grouping together neighboring points that exceeded a threshold, as described previously[25]. We then defined a summary statistics for each region based on the differences between nuclear and total counts of each nucleotide in the region as well as the trend of these counts. To assess the uncertainty of this procedure we generated a list of global null candidates by shuffling the sample labels and computed a summary statistic for these regions to form a null distribution. Then we ranked each potential candidate region by comparing their respective summary statistic to the null distribution to obtain an empirical p-value. The p-values were converted to q-values using the Benjamini-Hochberg approach.

Motif Analysis

MEME software package was used to find motifs enriched in differential regions. Specifically, we used the MEME function in the suite in the discriminative mode with DR sequences as the list of primary sequences and the other sequences in the pool as the controls. We ran MEME in different settings – OOPS and ANR - to ensure we found motifs that were repeating several times in a given DR and those only occurring once.

K-mer Enrichment

If sequence preferences are driven by more general sequence composition preferences that cannot be so easily represented by regular expression or position weight matrix motif models, then nuclear enrichment of DRs may be more effectively modeled by considering all k-mers. To this end, we performed a regression to assign weight coefficients to all k-mers for the DR sequences and non-DR sequences similar to the motif analysis using MEME as described previously. To avoid overfitting, we performed ridge regression[29], which minimizes not only the distance between model predictions and actual values but also the magnitude of the weights. We

299 chose the alpha parameter that varies the emphasis of these two competing objectives by
300 evaluating fivefold cross-validated mean squared error over a parameter grid.
301
302 **Conservation Analysis**
303 The phastCons and phyloP scores for the whole genome were downloaded from UCSC genome
304 browser. We extracted these scores for the DRs and shuffled control regions using a custom
305 script. In order to account for natural conservation differences between lncRNAs and mRNAs as
306 well as among different lncRNAs, the control regions were obtained by shuffling the DR
307 sequences using shuffleBed but ensuring the new regions fell within exons of the lncRNAs the
308 DRs were from. Finally, the scores were compared between DR and non-DR regions using the
309 Mann-Whitney test.
310
311 **ENCODE Fractionation RNA-Seq**
312 We downloaded the raw RNA-Seq reads for the nucleus and cytosolic compartments from the
313 ENCODE[30] website. These reads were quantified using kallisto to obtain TPMs and then the
314 nuclear/cytosolic TPMs of transcripts with the motif (found using the FIMO software) were
315 compared to all the other transcripts.
316
317 **Single molecule RNA fluorescence *in situ* hybridization (smRNA FISH)**
318 Briefly, 70-80% confluent 1x10^6 HeLa [ATCC® CCL-2™] cells were electroporated with 2 µg of
319 construct using the Amaxa® Cell Line Nucleofector® Kit R using program I-013, and cultured for
320 48 hours in LabTek v1 glass chambers. smRNA-FISH was performed using Biosearch
321 Technologies Stellaris® probes, as described previously (Reference). RNA probes targeting and
322 tiling the fsSox2 exon were conjugated to Quasar 570. Nuclei were visualized with 4,6-diamidino-
323 2-phenylindole (DAPI). Images were obtained using the Zeiss Cell Observer Live Cell microscope

at the Harvard Center for Biological Imaging. For each field of view, at least 40 slices (each plane: 0.24 µm) were imaged, and z-stacks were merged with maximum intensity projections (MIP). Sox2 foci were computationally-identified using the spot counting software StarSearch. To ensure robustness, the analysis was blinded and the person counting the spots did not know the identity of the samples. For each construct, fsSox2 foci within at least 150 cells were counted in biological duplicate.

Code availability

All the analysis in this paper was carried out using a custom package developed for the experiment called oligoGames. The package is currently hosted on GitHub - https://github.com/cshukla/oligoGames.

Data availability

All analyzed sequence data has been deposited in NCBI GEO under accession GSE98828.

References

1. Brown, C. J. *et al.* The human XIST gene: analysis of a 17 kb inactive X-specific RNA that contains conserved repeats and is highly localized within the nucleus. *Cell* **71,** 527–542 (1992).
2. Lee, J. T. & Bartolomei, M. S. X-Inactivation, Imprinting, and Long Noncoding RNAs in Health and Disease. *Cell* **152,** 1308–1323 (2013).
3. Gutschner, T. *et al.* The noncoding RNA MALAT1 is a critical regulator of the metastasis phenotype of lung cancer cells. *Cancer Res.* **73,** 1180–1189 (2013).
4. Clemson, C. M. *et al.* An Architectural Role for a Nuclear Non-coding RNA: NEAT1 RNA is Essential for the Structure of Paraspeckles. *Mol. Cell* **33,** 717–726 (2009).

5. Genome Regulation by Long Noncoding RNAs. *Annu. Rev. Biochem.* **81,** 145–166 (2012).

6. Tseng, Y.-Y. *et al.* PVT1 dependence in cancer with MYC copy-number increase. *Nature* **512,** 82–86 (2014).

7. Cabili, M. N. *et al.* Integrative annotation of human large intergenic noncoding RNAs reveals global properties and specific subclasses. *Genes Dev.* **25,** 1915–1927 (2011).

8. Derrien, T. *et al.* The GENCODE v7 catalog of human long noncoding RNAs: Analysis of their gene structure, evolution, and expression. *Genome Res.* **22,** 1775–1789 (2012).

9. Hacisuleyman, E., Shukla, C. J., Weiner, C. L. & Rinn, J. L. Function and evolution of local repeats in the Firre locus. *Nat. Commun.* **7,** (2016).

10. Zhang, B. *et al.* A novel RNA motif mediates the strict nuclear localization of a long non-coding RNA. *Mol. Cell. Biol.* MCB.01673-13 (2014). doi:10.1128/MCB.01673-13

11. Miyagawa, R. *et al.* Identification of cis- and trans-acting factors involved in the localization of MALAT-1 noncoding RNA to nuclear speckles. *RNA* **18,** 738–751 (2012).

12. Patwardhan, R. P. *et al.* High-resolution analysis of DNA regulatory elements by synthetic saturation mutagenesis. *Nat. Biotechnol.* **27,** 1173–1175 (2009).

13. Rosenberg, A. B., Patwardhan, R. P., Shendure, J. & Seelig, G. Learning the Sequence Determinants of Alternative Splicing from Millions of Random Sequences. *Cell* **163,** 698–711 (2015).

14. Melnikov, A. *et al.* Systematic dissection and optimization of inducible enhancers in human cells using a massively parallel reporter assay. *Nat. Biotechnol.* **30,** 271–277 (2012).

15. Ernst, J. *et al.* Genome-scale high-resolution mapping of activating and repressive nucleotides in regulatory regions. *Nat. Biotechnol.* **34,** 1180–1190 (2016).

16. Martin, K. C. & Ephrussi, A. mRNA Localization: Gene Expression in the Spatial Dimension. *Cell* **136,** 719–730 (2009).

17. Paquin, N. & Chartrand, P. Local regulation of mRNA translation: new insights from the bud. *Trends Cell Biol.* **18,** 105–111 (2008).

18. Bullock, S. L. & Ish-Horowicz, D. Conserved signals and machinery for RNA transport in Drosophila oogenesis and embryogenesis. *Nature* **414,** 611–616 (2001).

19. Davis, I. & Ish-Horowicz, D. Apical localization of pair-rule transcripts requires 3' sequences and limits protein diffusion in the Drosophila blastoderm embryo. *Cell* **67,** 927–940 (1991).

20. Johnstone, O. & Lasko, P. Translational regulation and RNA localization in Drosophila oocytes and embryos. *Annu. Rev. Genet.* **35,** 365–406 (2001).

21. Lin, A. C. & Holt, C. E. Local translation and directional steering in axons. *EMBO J.* **26,** 3729–3736 (2007).

22. Rinn, J. & Guttman, M. RNA and dynamic nuclear organization. *Science* **345,** 1240–1241 (2014).

23. Oikonomou, P., Goodarzi, H. & Tavazoie, S. Systematic Identification of Regulatory Elements in Conserved 3′ UTRs of Human Transcripts. *Cell Rep.* **7,** 281–292 (2014).

24. Cabili, M. N. *et al.* Localization and abundance analysis of human lncRNAs at single-cell and single-molecule resolution. *Genome Biol.* **16,** 20 (2015).

25. Jaffe, A. E. *et al.* Bump hunting to identify differentially methylated regions in epigenetic epidemiology studies. *Int. J. Epidemiol.* **41,** 200–209 (2012).

26. Siepel, A. *et al.* Evolutionarily conserved elements in vertebrate, insect, worm, and yeast genomes. *Genome Res.* **15,** 1034–1050 (2005).

27. Siepel, A., Pollard, K. S. & Haussler, D. New Methods for Detecting Lineage-specific Selection. in *Proceedings of the 10th Annual International Conference on Research in Computational Molecular Biology* 190–205 (Springer-Verlag, 2006). doi:10.1007/11732990_17

398 28. Machanick, P. & Bailey, T. L. MEME-ChIP: motif analysis of large DNA datasets.
399 *Bioinforma. Oxf. Engl.* **27,** 1696–1697 (2011).
400 29. Le Cessie, S. & Van Houwelingen, J. C. Ridge Estimators in Logistic Regression. *J. R.*
401 *Stat. Soc. Ser. C Appl. Stat.* **41,** 191–201 (1992).
402 30. An Integrated Encyclopedia of DNA Elements in the Human Genome. *Nature* **489,** 57–
403 74 (2012).
404 31. Levesque, M. J. & Raj, A. Single-chromosome transcriptional profiling reveals
405 chromosomal gene expression regulation. *Nat. Methods* **10,** 246–248 (2013).
406 32. Zhao, S. & Fernald, R. D. Comprehensive algorithm for quantitative real-time
407 polymerase chain reaction. *J. Comput. Biol. J. Comput. Mol. Cell Biol.* **12,** 1047–1064 (2005).
408
409 **Supplementary Information** is available in the online version of the paper.
410
411 **Acknowledgements**
412 The authors would like to thank Doug Richardson and Sven Terclavers at Harvard Center for
413 Biological Imaging for assistance with imaging, Ezgi Haceysuleyman for advice on smRNA-FISH
414 and Bauer Sequencing Facility at Harvard University for assistance with the sequencing. CJS
415 would like to acknowledge Alejandro Reyes for advice on writing the manuscript and analyzing
416 the data. The authors would like to thank everyone in the Rinn and Irizarry lab for their advice and
417 insightful comments throughout this work. This work was supported by NIH grants R01GM083084
418 and R01HG005220 to RAI as well as NIH grants U01DA040612-01 and P01GM099117 to JLR.
419
420 **Author Contributions**
421 These authors contributed equally to this work.
422 Philipp G Maass, John L Rinn

Author Information

Tables

Extended Data Table 1: A table describing the meta data of the oligo pool used in this work.

Extended Data Table 2: A table describing the 109 DRs discovered in this work.

Figure Legends

Figure 1. A Massively Parallel Reporter Assay to identify RNA nuclear enrichment signals. **A**. Experimental overview. *Far left*: oligonucleotide pool design. Double-stranded DNA (dsDNA) oligonucleotides were designed by computationally scanning 38 parental lncRNA transcripts ("lncRNA cDNAs," **Extended Data Table 1**) in 110 bp windows, with 10 bp spacing between sequential oligos. These lncRNA-derived "Variable Sequences" (gray) were appended with unique barcodes and primer binding sides, resulting in a pool of 11,969 oligos (**Supplementary Data 1**). The vertical lines in the lncRNA denote splice junctions. *Second from left:* schematic summarizing the design of each pool oligonucleotide. *Second from right:* Reporter design. The oligonucleotide pool was cloned into a reporter plasmid as a transcriptional fusion at the 3´-terminus of the fsSox2 gene. pA: polyadenylation sequence *Far right:* MPRA workflow. The Sox2~oligo reporter pool is transiently transfected into HeLa cells. Following 48h of expression, cells are subsequently fractionated to isolate nuclei, and the nuclear enrichment of each pool member is quantified by targeted RNA sequencing (*not shown*). Matched whole-cell lysates from unfractionated cells serve as controls. **B**–**C.** Differential Region-calling correctly identifies nuclear retention elements in *MALAT1*. Solid lines: per-nucleotide abundances in the nuclear (red) and

whole-cell (gray) fractions, modeled for each position along the *MALAT1* transcript, based on the aggregate behavior of all oligos containing that nucleotide (*Methods*). Shaded regions: standard deviations. Median values for six biological replicates are shown. **D.** Boxplot comparing the nuclear enrichment for all nucleotides within differential regions ("DRs"), relative to all the other nucleotides surveyed ("Non DRs"). *P*-value: Mann Whitney Test.

Figure 2. Novel lncRNA nuclear enrichment signals. A–E. Identification of Differential Regions within lncRNAs with different subcellular localization patterns. Data are depicted as in **Figure 1C**. Established subcellular localization patterns range from: **A**. those occupying a single, prominent nuclear focus (*ANRIL,* FISH Class 1), to: **E**. those exhibiting a diffuse, mostly cytosolic pattern (*NR*_024412, FISH Class 5)[24]. **F**. The number of Differential Regions discovered within lncRNAs from each FISH Class correlates with that class's degree of nuclear localization. **G**. Differential Regions are more highly conserved than are most lncRNA sequences. Cumulative distribution function (CDF) of phastCons scores comparing nucleotides within Differential Regions (*red*), to all other nucleotides within the oligo pool (*gray*). *P*-value: Mann Whitney Test.

Figure 3. Motifs enriched in lncRNA nuclear enrichment signals. A. Position Weight Matrix (PWM) for a novel 57 nt motif enriched within the DRs of lncRNA *XIST,* discovered using MEME[28]. E-value < 0.05 **B**. Occurrences of this motif throughout the *XIST* locus. **C.** Multiple sequence alignment of the incidences of this *XIST* motif (*colored nucleotides*) within Differential Regions. Adjoining sequences are colored in gray. **D**. PWM for a novel C-rich 15 nt motif enriched within the DR's of 21 different lncRNAs, discovered using MEME. E-value < 0.05 **E**. The occurrences of this motif throughout the *MALAT1* locus. **F**. Multiple sequence alignment of different instances of this motif (*colored nucleotides*), as they appear in the Differential Regions of the indicated lncRNAs. **G**. Oligos bearing the novel motifs described in **A**–**F** and **Extended Data Figure 4** are

473 significantly enriched in nuclear fractions, relative to all other oligos in the MPRA pool. *P*-value:
474 Mann Whitney Test. **H–I** . Novel nuclear enrichment motifs influence the localization of
475 endogenous human transcripts. CDF plot comparing the nuclear enrichment of all human
476 transcripts with at least one occurrence of our discovered motifs, relative to all other transcripts,
477 in HeLa and A549 cells[30]. *P*-value: Mann Whitney Test.
478
479 **Figure 4. Differential Regions are sufficient to redirect RNA subcellular localization A-B**.
480 Representative *XIST* and C-Rich motif regions and novel Differential Regions from lncRNAs
481 *TUG1* and *XIST* that are examined in **B**–**D**. Data depicted as in **Figure 1C**. **B-C.** Experimental
482 overview of single-molecule RNA FISH (smRNA–FISH) experiments. Sox2 reporter constructs
483 fused to individual motifs are transiently expressed in HeLa cells, and the resulting fusion
484 transcripts are imaged using a common probe set targeting fsSox2[9,31]. Representative smRNA-
485 FISH images demonstrating the behavior of (*left*) the unmodified fsSox2 reporter, (*middle*) the
486 reporter fused to three tandem instance of the *XIST*-derived motif ("Motif1"), and (*right*) the
487 reporter fused to three tandem instances of the C-rich motif ("Motif2"). Scale bars are the same
488 for all images. Blue: Hoechst 33342 Representative smRNA-FISH images of HeLa cells
489 transiently expressing the indicated Sox2 reporter constructs: unmodified fsSox2, MALAT1
490 Region M (*second from left)*, TUG1 Differential Region (*second from right)* and XIST Differential
491 Region (*right most)*. Data were collected using the experimental scheme outlined above. Scale
492 bars are the same for all images. **E.** Quantification of the apparent nuclear localization of Sox2
493 reporter constructs, fused to the indicated Motifs, as observed using smRNA-FISH (*Methods) P*-
494 value: Mann Whitney Test.
495
496
497

498 **Figure 1**

499

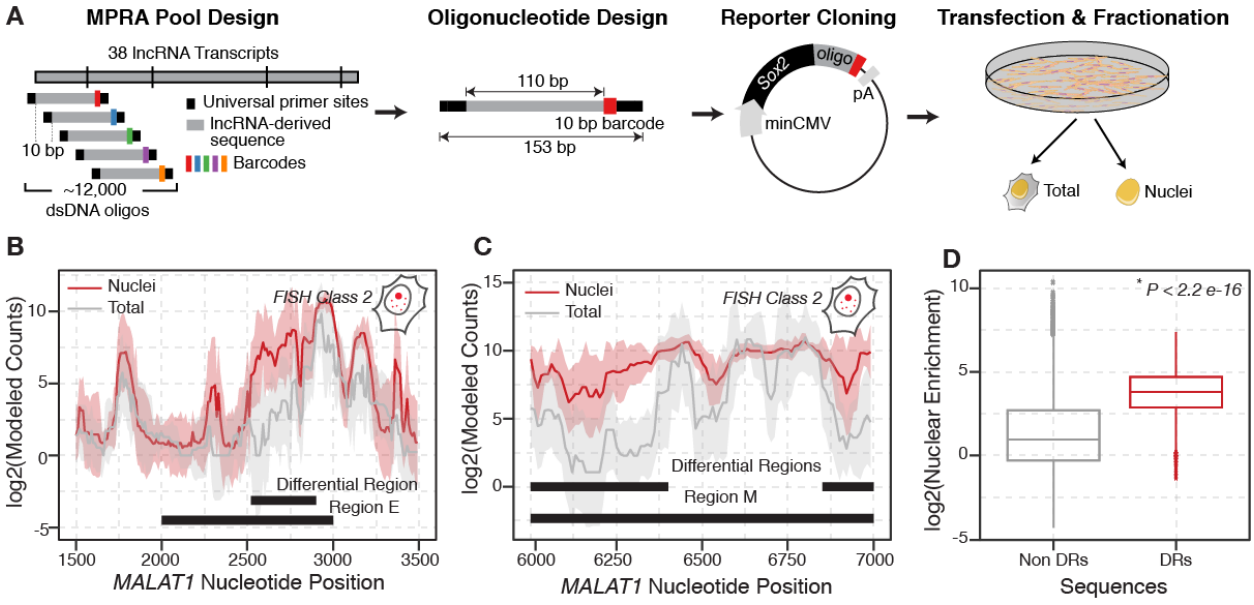

500

501

502

503

504

505

506

507

508

509

510

511

512

513

514

Figure 2

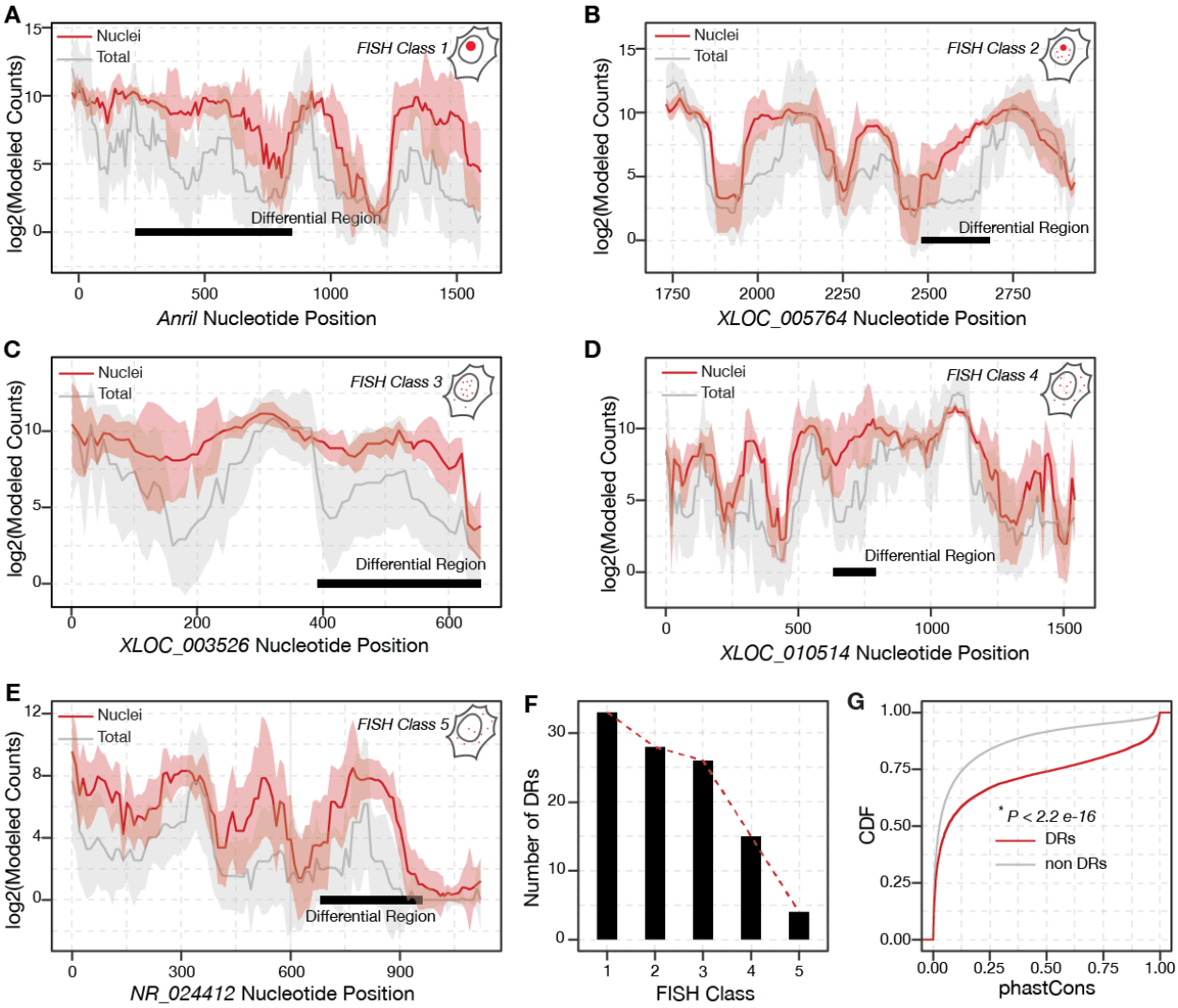

Figure 3

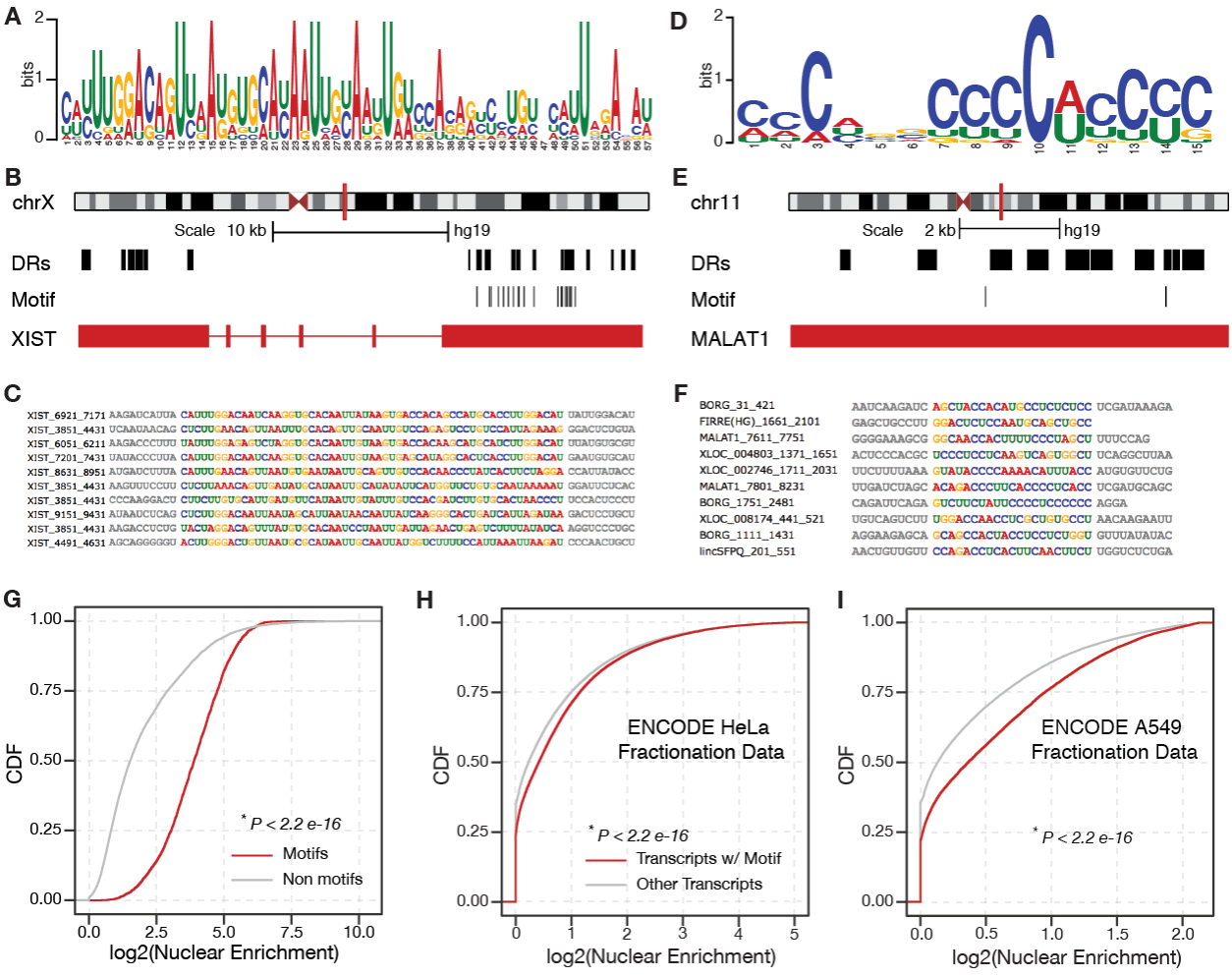

Figure 4

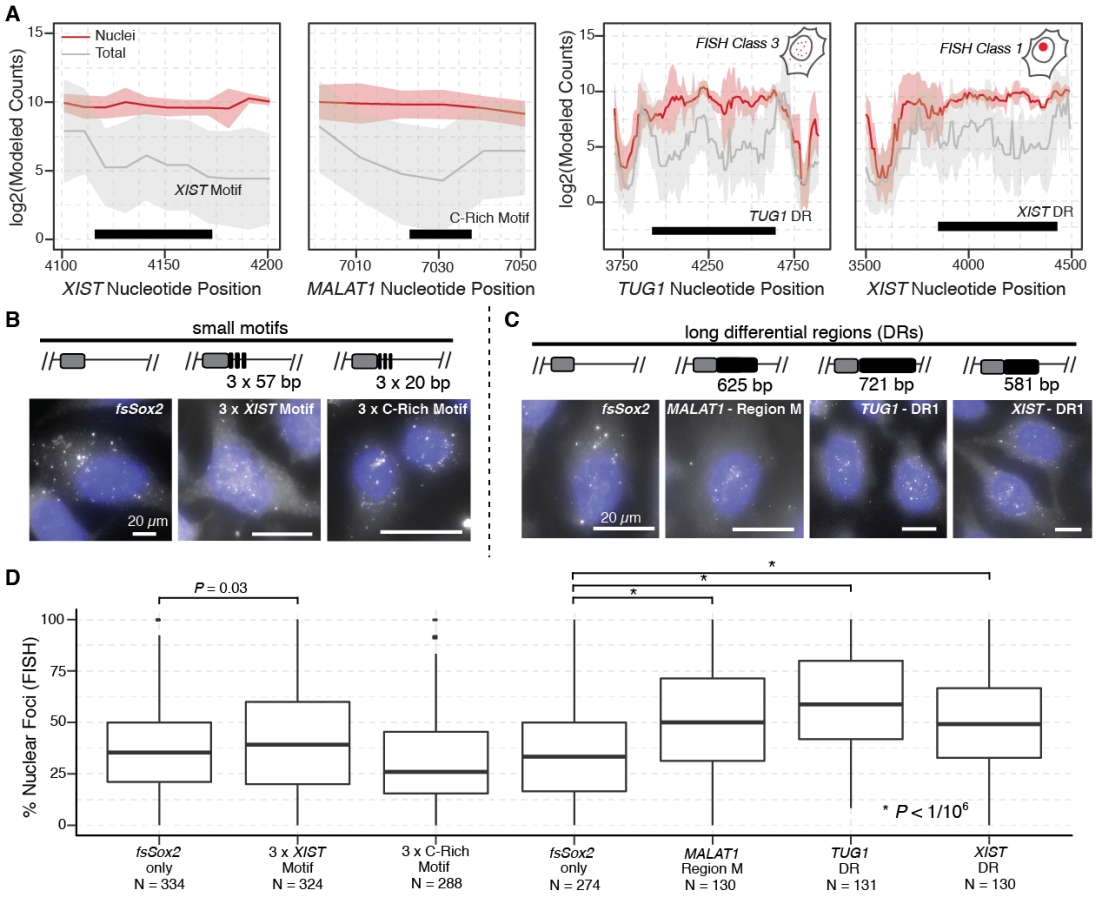

548 **Extended Data Figure Legends:**

549

550 **Figure 1. Computational pipeline to identify nuclear enrichment signals from MPRA data.**
551 **A.** Post fractionation, RNA from the nucleus and whole cell lysate is extracted. Using the universal
552 primer sequences, the oligos are amplified in a targeted manner to make the library which is sent
553 for sequencing. **B.** The first step in the analysis process is to map the reads back to the oligo pool.
554 Due to the dense tiling of lncRNAs in our pool, we ensure there is a perfect match between the
555 first 10 nucleotides of the read and the barcode sequence to 'map' the read. Next, we require the
556 upstream 90 bps to only have 2 mismatches to guarantee robusteness of the mapping procedure.
557 This step is performed by the 'mapReads' function in our package which gives a table of counts
558 for each oligo as the output. This counts table is subsequently normalized for library size using
559 the 'normCounts' table. We provide this normalized counts table along with the data on GEO **C.**
560 Based on the normalized counts for each oligo, counts for each nucleotide are modeled next. As
561 shown in the schematic, if a nucleotide 'A' overlaps with oligos i_1, i_2, i_3 and i_4 the counts for the
562 nucleotide A are modeled by taking the median of counts for each of the individual oligos i_1 – i_4.
563 We use the 'modelNucCounts' function in our package for this and get a counts table for each
564 nucleotide in all the 12 samples (6 nuclei and 6 total) as the output (**Supplementary File 2**). **D.**
565 Using the nucleotide counts table, we infer differential regions by 1). Finding candidate regions
566 and assigning a summary statistic to each one of them and 2). Generating null candidates by
567 permuting sample labels and using them to assign an empirical p-value to our candidate regions
568 from Step 1. Please see Methods for more details (*Inset*) A distribution of the summary statitistic
569 generated for the data we present in the paper – the red line shows the cutoff used to decide the
570 'significant' candidates.

571

572 **Figure 2. Quality Control for Various MPRA Steps** Since the MPRA has several steps, we
573 used controls at every stage to make sure the assay was working as designed **A.** The distribution
574 of oligo's in our cloned plasmid pool. We see that (i). there is very little jackpotting (just a single
575 peak showing uniform counts for several different oligos) and (ii). we have almost the entire pool
576 represented (very small bump at zero counts). **B**. The nuclear enrichment of *NEAT1*, *GAPDH* and
577 *SNHG5* as determined by qRT-PCR (*Methods*). The error bars represent standard deviation for
578 each measurement. We see that the lncRNA *NEAT1* (green) is enriched in the nuclear fraction
579 as expected while The 'control' represents the enrichment of the genes in untransfected cells
580 (*Inset)* The median enrichment of the genes across all 6 replicates. **C.** A representative image of
581 HeLa cells co-transfected with a GFP plasmid using the protocol outlined in Methods showing
582 that we achieve a high transfection efficiency. **D.** The number of oligos 'missing' (i.e. with zero
583 counts) from each of our 12 samples. We see that we recover >70% of our initial pool in each
584 sample and looking across the 6 samples for nucleus and total, only 0.2% oligos (i.e. ~25 oligos)
585 are missing from the nuclear samples and ~0.4% (i.e. ~50 oligos) are missing from the total
586 sample.
587
588 **Figure 3 Mapping Rates for our different samples** A bar plot showing the mapping percentage
589 for all reads of different samples from nuclear fraction (N) and total fraction (T). We show the
590 mapping rates separately for the 2 technical replicates (TR) and each of the 6 biological replicates
591 (BR).
592
593 **Figure 4 Difference between counts of technical replicates** A boxplot showing difference
594 between counts of same oligo between the 2 technical replicates. We see that many oligos show
595 very low difference in counts among technical replicates and thus there is very low technical
596 variance.

Figure 5 Biological Validation of MPRA Using the *FIRRE* locus Similar to the MALAT1 Region M and Region E we used to ensure our MPRA was working robustly, we can also use the RRD region from the FIRRE locus. **A.** The MPRA recapitulates the function of known RNA nuclear retention element – RRD. Since, the experiment was performed in human cells, we expect RRD derived from human *FIRRE* to positively influence nuclear enrichment while the RRD derived from mouse *FIRRE* will not influence nuclear enrichment of fsSox2. Here, we show a CDF plot of the nucleotides overlapping human RRD, mouse RRD and other nucleotides in the human and mouse *FIRRE* loci. *P*-value: Mann Whitney Test. **B.** Differential Region-calling correctly identifies nuclear retention elements in *FIRRE*. Solid lines: per-nucleotide abundances in the nuclear (red) and whole-cell (gray) fractions, modeled for each position along the *FIRRE* transcript, based on the aggregate behavior of all oligos containing that nucleotide (*Methods*). Shaded regions: standard deviations. Median values for six biological replicates are shown.

Figure 6 Sequence Features of Differential Regions A. A boxplot showing the length distribution of the differential regions generated by our method. We see that most of our differential regions are longer than 110 bp oligo nucleotide we started with. **B.** A scatter plot showing the relationship between number of differential regions in a lncRNA (X-axis) and the length of the lncRNA (Y-axis). The blue line shows the loess fit and the shaded region is the confidence interval around the fit. **C.** A bar graph comparing GC content of DRs and non DRs which shows there is no noticeable difference in GC content.

Figure 7 Motifs enriched in lncRNA nuclear enrichment signals. A-D. Position Weight Matrix (PWM) for a novel motifs enriched in DR sequences found using MEME software. While motif in panel A is similar to the C-rich motif in **Figure 4D** the other 3 motifs are found in XIST and similar

to the XIST specific motif in **Figure 4A** E-Value < 0.05. **E.** k-mers mildply predictive of DR found using ridge regression. The color describes the weight of the kmer assigned by the ridge regression algorithm (*Methods)*.

Figure 8 Novel C-rich motif can influence the localization of endogenous human transcripts. CDF plot comparing the nuclear enrichment of all human transcripts with at least one occurrence of our discovered motifs, relative to all other transcripts, in all ENCODE Tier 2 cells[30]. *P*-value: Mann Whitney Test.

Extended Data Figure 1

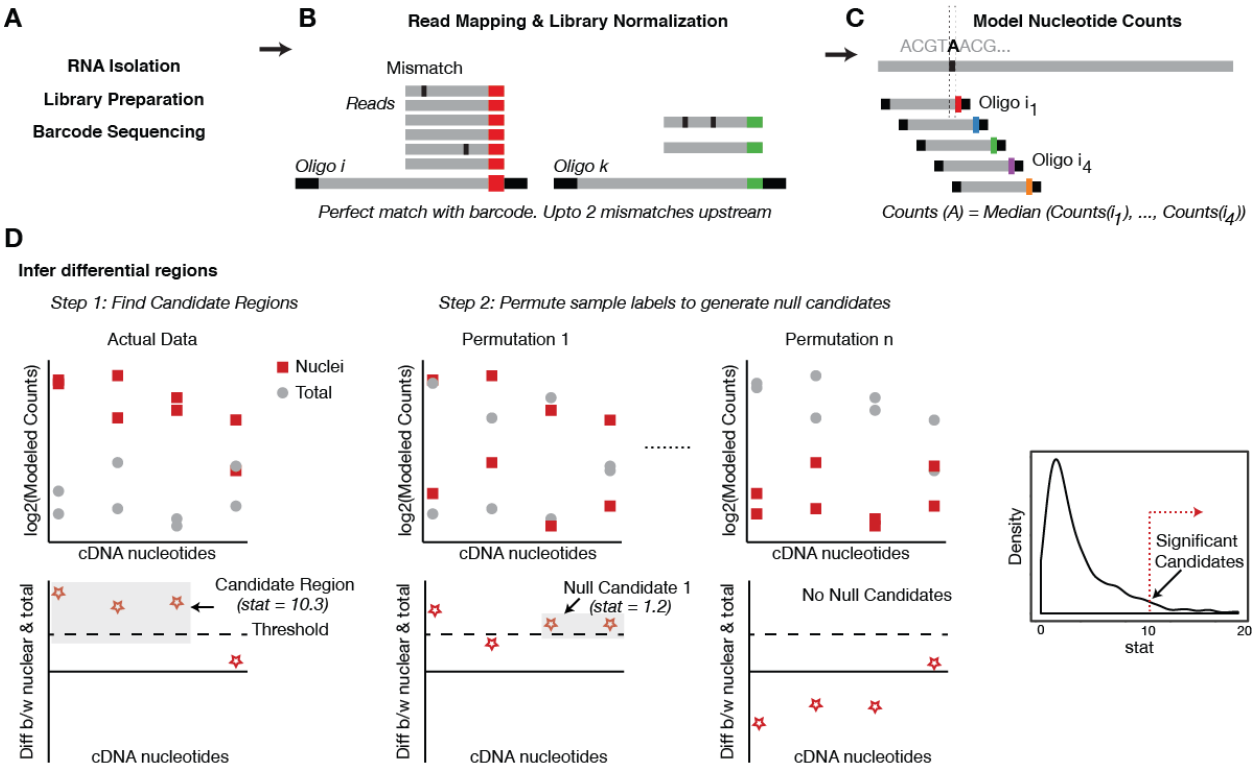

Extended Data Figure 2

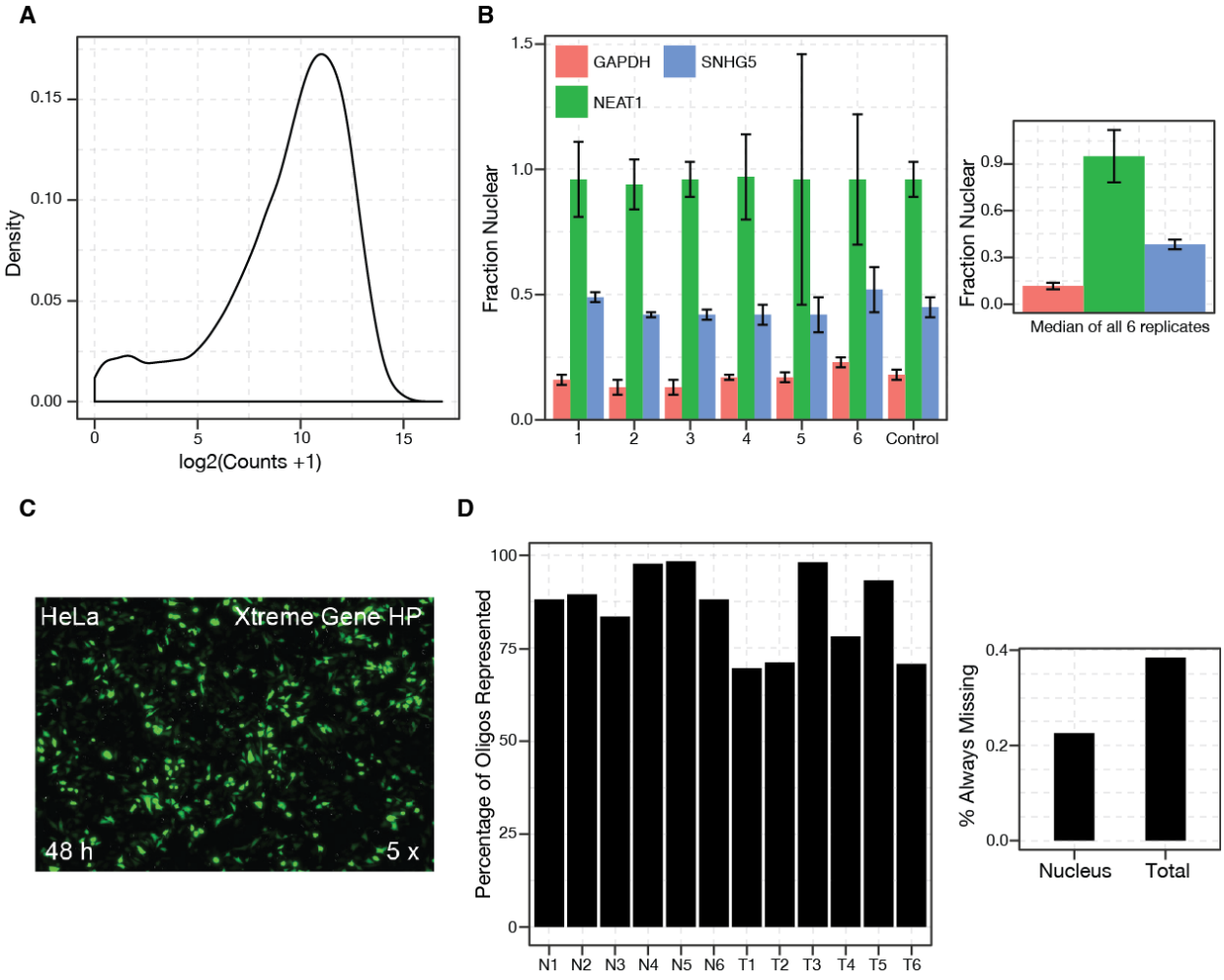

672 **Extended Data Figure 3**

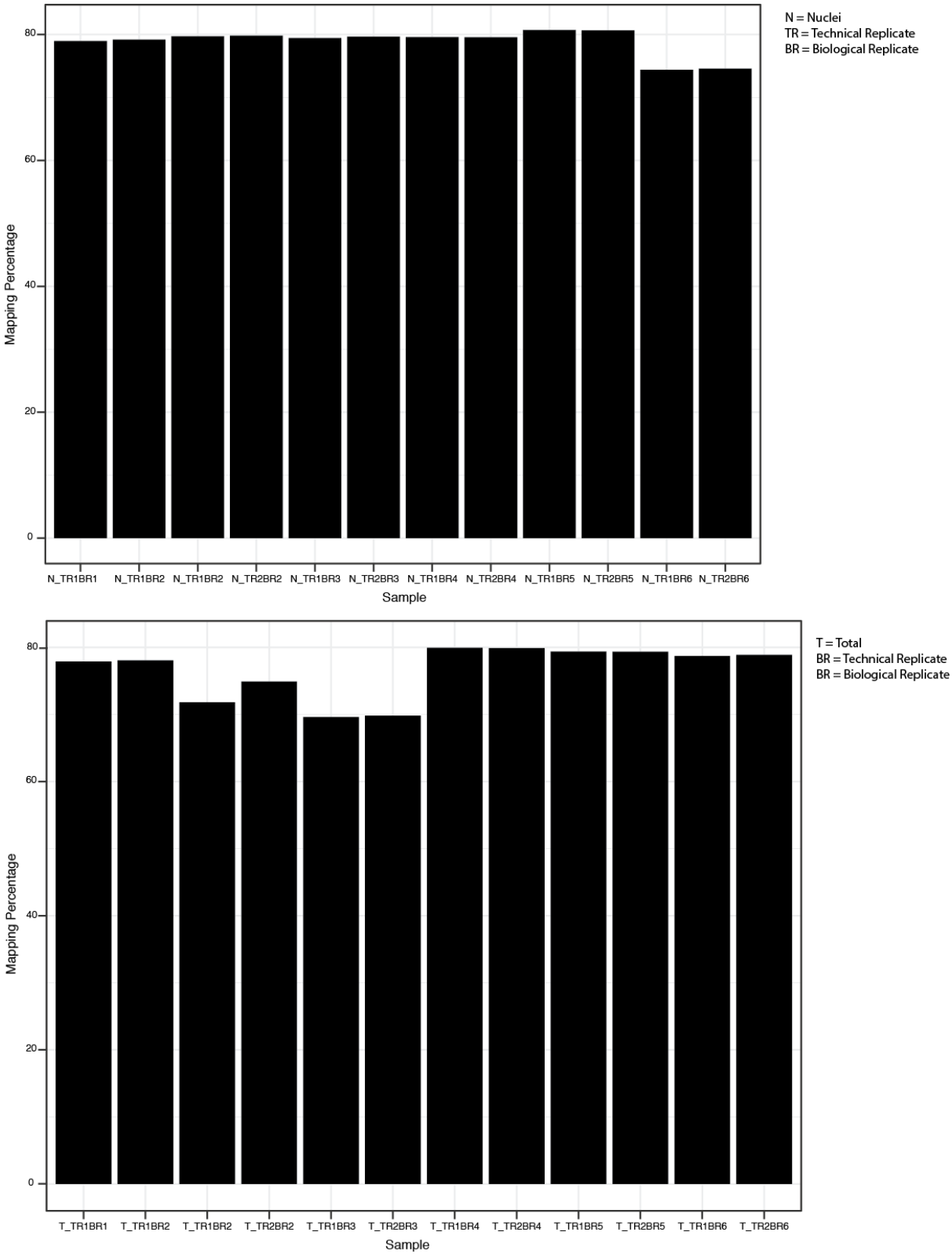

673

674 **Extended Data Figure 4**

675

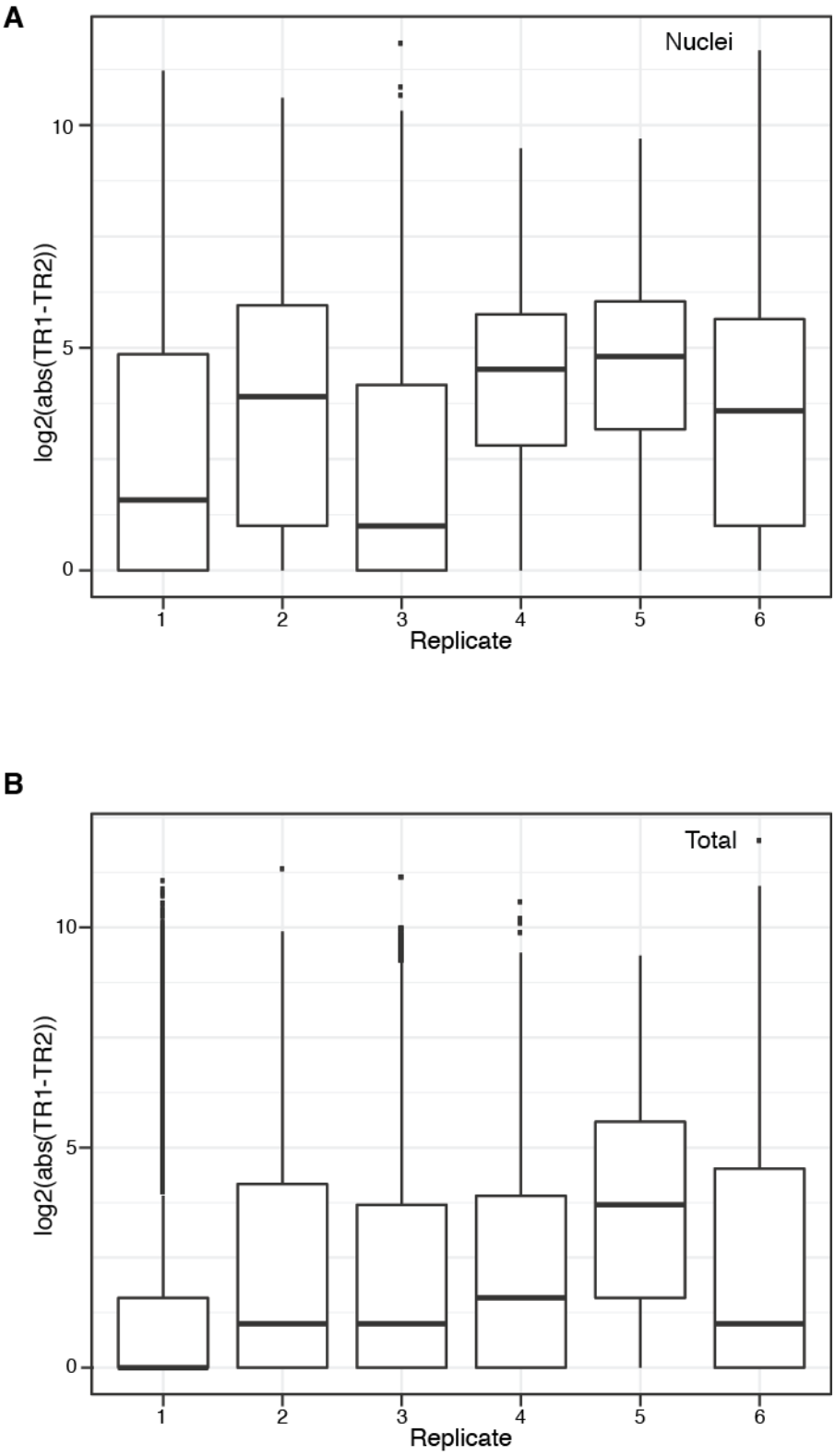

676

677 **Extended Data Figure 5**

678

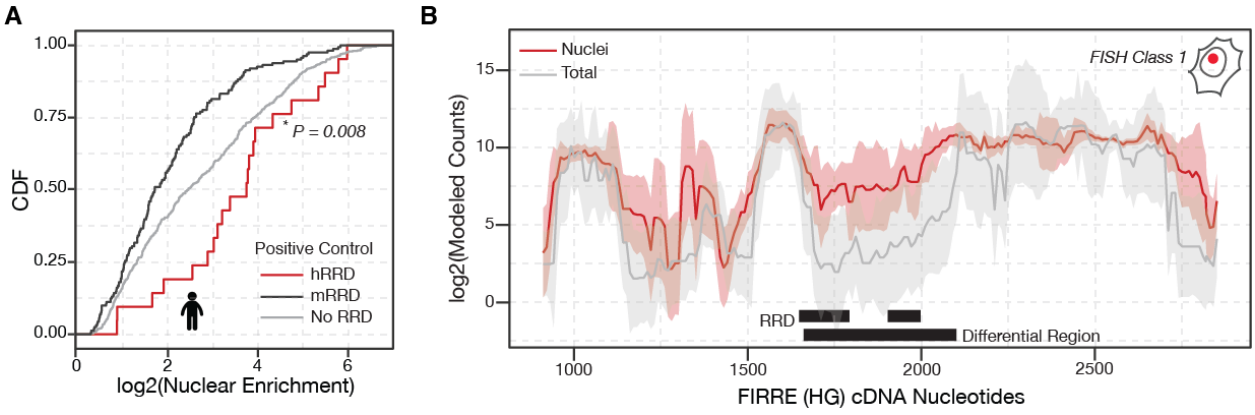

679

680

681

682

683

684

685

686

687

688

689

690

691

692

693

694

695

Extended Data Figure 6

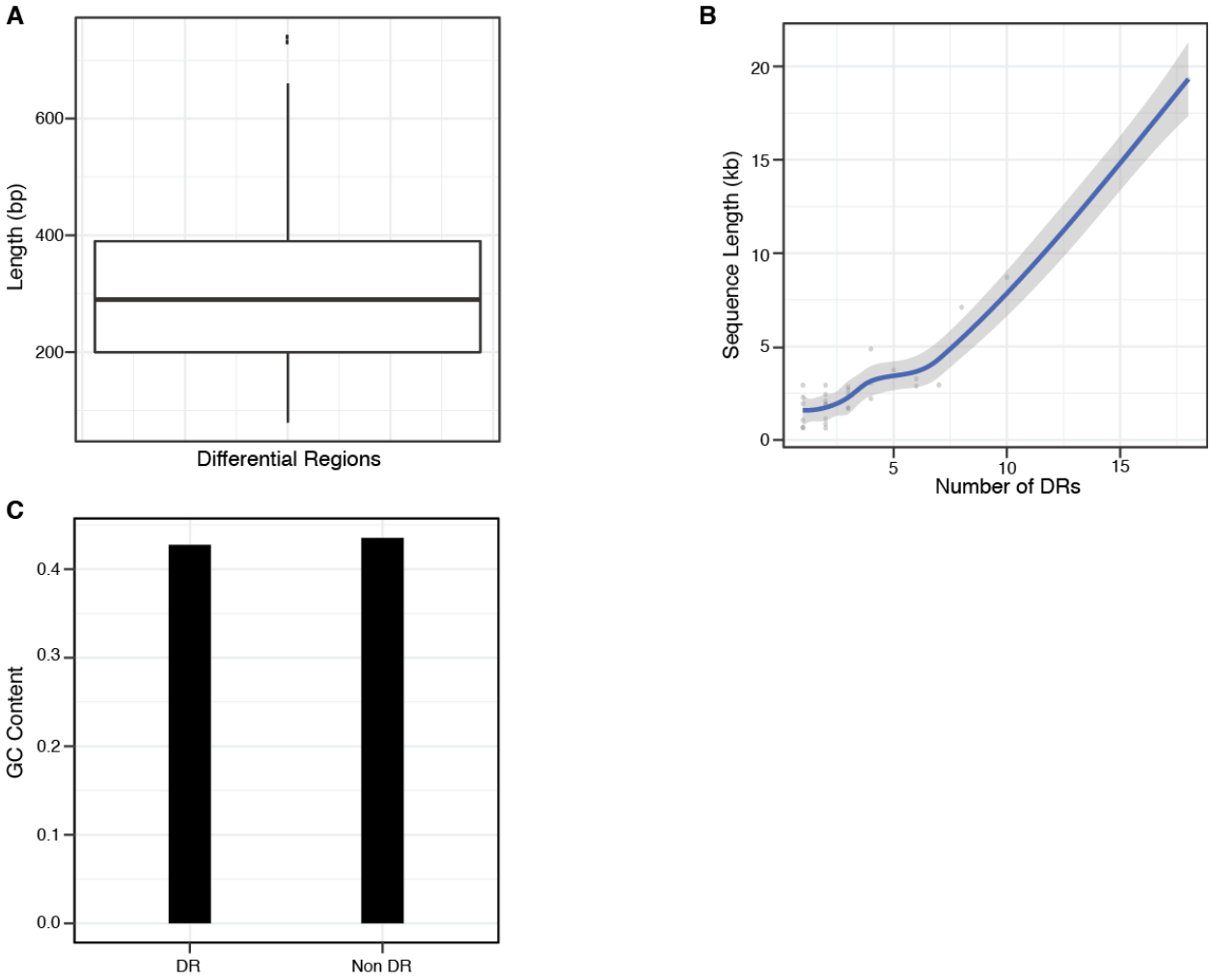

Extended Data Figure 7

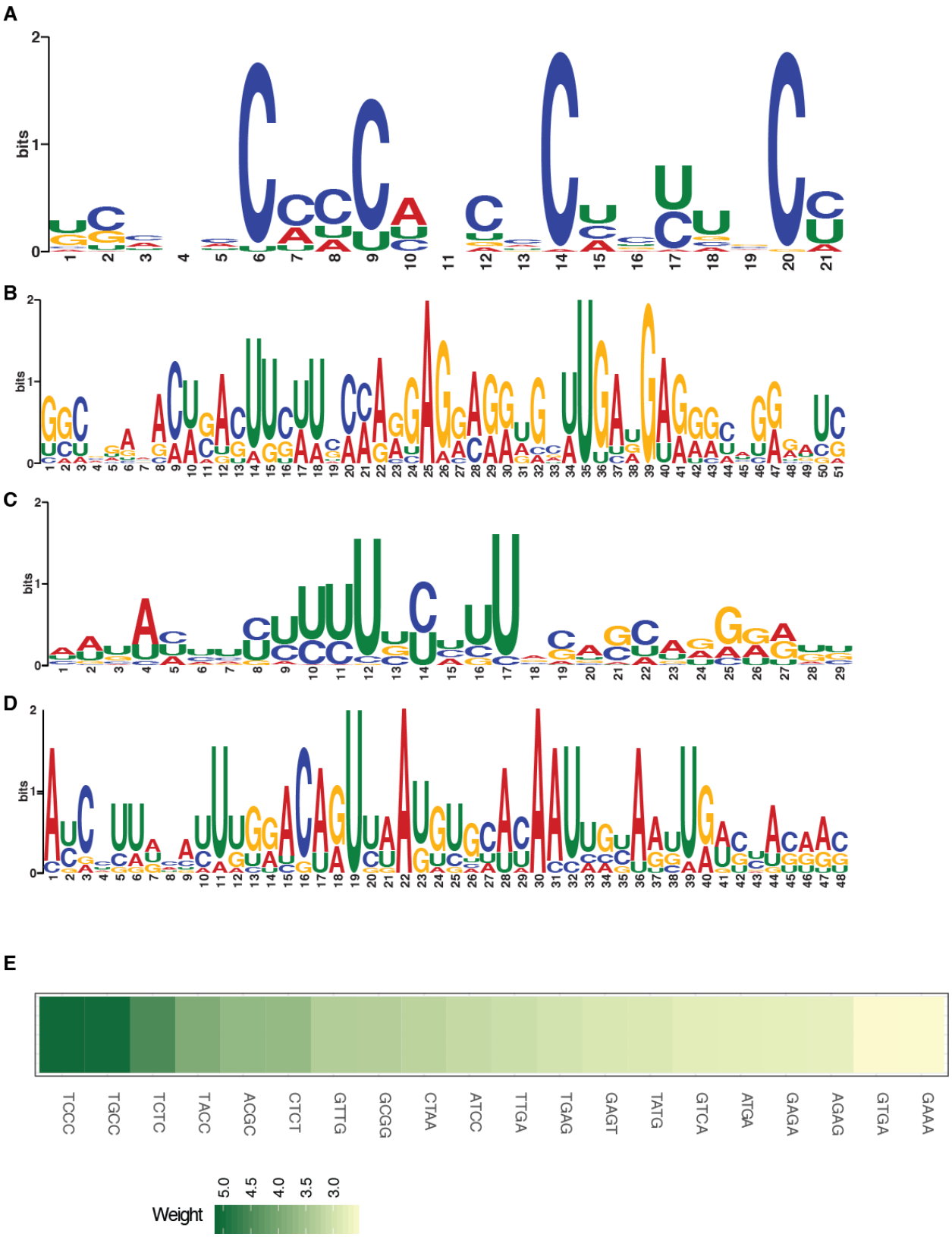

Extended Data Figure 8

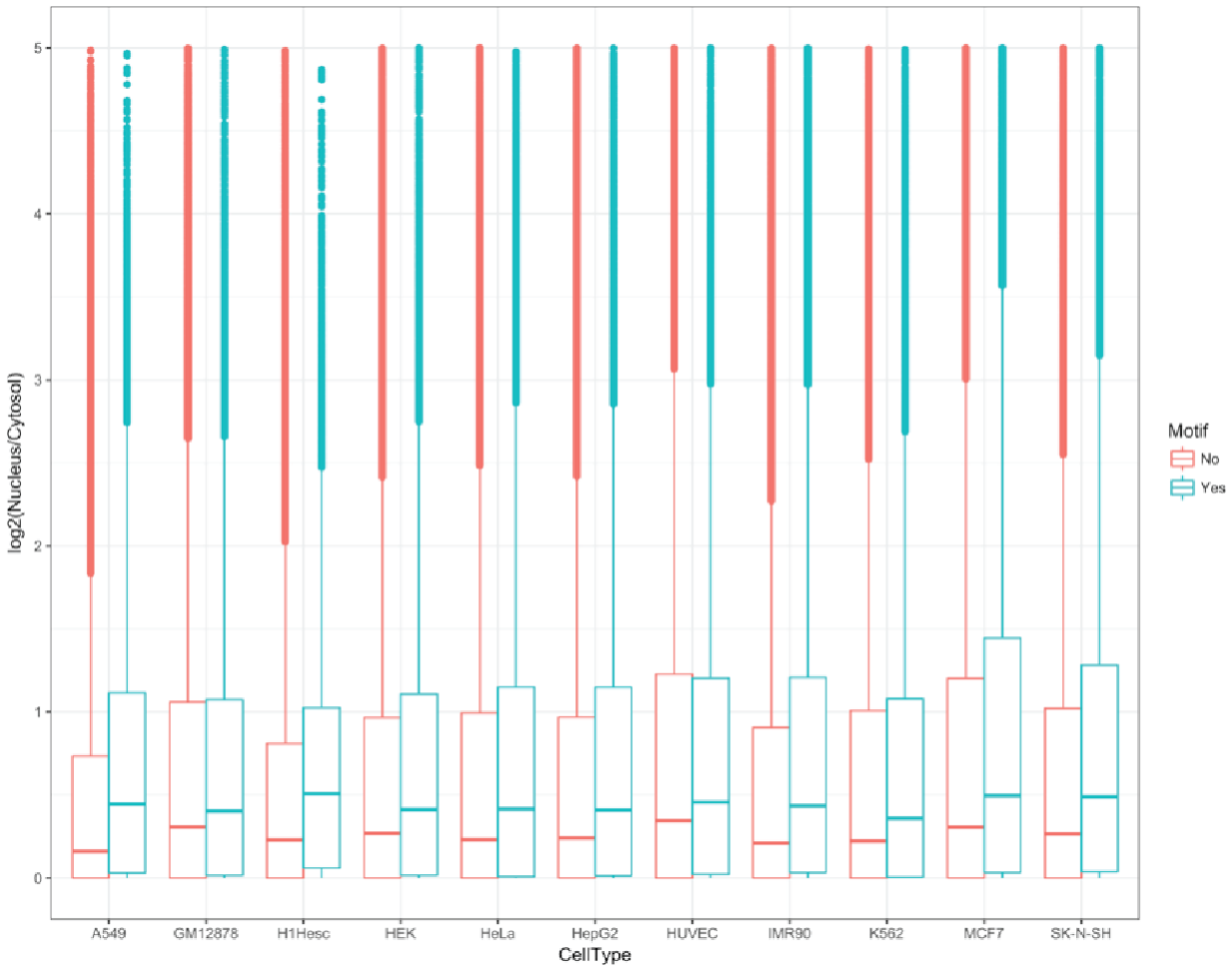

720 **Extended Data Table 1**

721

txnNum	seqid	name1	name2	startIndex	numOfOligos	seqLen	fishClass	window
1	76_1_75	ANCR	NR_024031	0	76	855	4	10
2	234_2_157	Anril	NR_003529	75	158	1676	1	10
3	509_3_274	BORG	AB010885	232	275	2846	*	10
4	708_4_198	ENST00000606034.1	ENST00000606034.1	506	199	2086	*	10
5	991_5_282	FIRRE(HG)	NR_026975	704	283	2928	1	10
6	1469_6_477	FIRRE(MM)	NR_026976	986	478	4872	1	10
7	1523_7_53	GAS5	NR_002578	1463	54	632	2	10
8	2384_8_860	MALAT1	NR_002819	1516	861	8708	2	10
9	2547_9_162	Meg3	NR_033358	2376	163	1722	2	10
10	2911_10_363	NEAT1	NR_028272	2538	364	3735	2	10
11	3014_11_102	NR_024412	NR_024412	2901	103	1127	5	10
12	3250_12_235	NR_029435	NR_029435	3003	236	2457	3	10
13	3286_13_35	TERC	NR_001566	3238	36	451	2	10
14	3987_14_700	TUG1	NR_002323	3273	701	7104	3	10
15	5905_15_1917	XIST	NR_001564	3973	1918	19280	1	10
16	5961_16_55	XLOC_002094	TCONS_00005148	5890	56	660	4	10
17	6057_17_95	XLOC_002408	NR_040001	5945	96	1058	4	10
18	6375_18_317	XLOC_002746	NR_028301	6040	318	3278	3	10
19	6431_19_55	XLOC_003526	TCONS_00007523	6357	56	653	3	10
20	6494_20_62	XLOC_004456	NR_039993	6412	63	730	3	10
21	6727_21_232	XLOC_004803	TCONS_00010926	6474	233	2429	4	10
22	7022_22_294	XLOC_005151	DB2.2_TCONS_00023484	6706	295	3047	1	10
23	7306_23_283	XLOC_005764	NR_026807	7000	284	2933	2	10
24	7488_24_181	XLOC_006922	NR_003367	7283	182	1918	1	10
25	7767_25_278	XLOC_008174	NR_015353	7464	279	2886	4	10
26	7825_26_57	XLOC_009233	NR_038903	7742	58	673	3	10
27	8005_27_179	XLOC_009702	NR_040245	7799	180	1895	4	10
28	8216_28_210	XLOC_010017	NR_028045	7978	211	2208	3	10
29	8401_29_184	XLOC_010514	NR_044993	8188	185	1942	4	10
30	8619_30_217	XLOC_011185	NR_023915	8372	218	2280	4	10
31	8799_31_179	XLOC_011226	NR_026757	8589	180	1894	4	10
32	8854_32_54	XLOC_011950	NR_034106	8768	55	650	4	10

33	9053_33_198	XLOC_012599	NR_033770	8822	199	2090	5	10
34	9123_34_69	XLOC_L2_008203	NR_015395	9020	70	793	4	10
35	9134_35_10	lincFOXF1	NR_036444	9089	11	206	4	10
36	9419_36_284	lincMKLN1_A1	NR_015431	9099	285	2948	2	10
37	9678_37_258	lincSFPQ	uc001byq.3	9383	259	2685	3	10
38	11969_38_2290	kcnq1ot1	NR_002728	9679	2291	91671	1	40

742 **Extended Data Table 2**

743

chr	start	end	indexStart	indexEnd	length	stat	pval	qval
TUG1	3921	4641	3822	3894	73	19.78425693	1.37E-04	0.032707591
XIST	3851	4431	4527	4585	59	18.93234834	1.37E-04	0.032707591
BORG	1751	2481	432	505	74	18.02645224	1.92E-04	0.032707591
XLOC_005151	591	981	7015	7054	40	17.56243041	1.92E-04	0.032707591
NEAT1	1221	1561	2769	2803	35	16.33411768	3.01E-04	0.035043848
FIRRE(MM)	71	561	1054	1103	50	16.23299636	3.29E-04	0.035043848
FIRRE(MM)	1551	2201	1202	1267	66	15.82546972	3.84E-04	0.035043848
MALAT1	5471	5951	2148	2196	49	15.41161228	4.11E-04	0.035043848
MALAT1	5971	6401	2198	2241	44	15.08001304	4.93E-04	0.037380104
TUG1	2521	2931	3682	3723	42	14.64829348	6.03E-04	0.041118115
Anril	251	871	113	175	63	14.18387442	7.95E-04	0.044568586
XIST	18601	19141	6002	6056	55	13.83398428	8.22E-04	0.044568586
XLOC_010017	81	311	8308	8331	24	13.78124507	8.50E-04	0.044568586
XIST	951	1191	4237	4261	25	13.63602836	9.59E-04	0.045790628
MALAT1	4711	5121	2072	2113	42	13.55591772	0.001068786	0.045790628
TUG1	3101	3501	3740	3780	41	13.4734457	0.001123596	0.045790628
lincMKLN1_A1	1871	2341	9701	9748	48	13.46301764	0.001151	0.045790628
XIST	1601	1731	4302	4315	14	13.30739043	0.001315429	0.045790628
XLOC_009702	21	361	8111	8145	35	13.12962204	0.001342834	0.045790628
FIRRE(HG)	1661	2101	919	963	45	13.09486481	0.001342834	0.045790628
XLOC_002746	1131	1661	6356	6409	54	13.04185855	0.001425048	0.045946378
ANCR	571	851	58	87	30	12.98651091	0.001507262	0.045946378
XLOC_012599	151	621	9217	9264	48	12.90796589	0.001616881	0.045946378
XIST	8631	8951	5005	5037	33	12.84592969	0.001616881	0.045946378
XLOC_002746	1711	2031	6414	6446	33	12.53548694	0.001890929	0.051584544
BORG	31	421	260	299	40	12.18400479	0.002329405	0.056070156
XIST	7201	7431	4862	4885	24	12.15842074	0.002329405	0.056070156
XLOC_005151	41	161	6960	6972	13	12.13686517	0.00235681	0.056070156
lincSFPQ	201	551	9830	9865	36	12.04103864	0.002439024	0.056070156
TUG1	6221	6561	4052	4086	35	11.96916084	0.002548643	0.056070156
XIST	15631	16081	5705	5750	46	11.96071375	0.002548643	0.056070156
XLOC_002746	2791	3091	6522	6552	31	11.77047577	0.002877501	0.059716996
XLOC_005151	1331	1691	7089	7125	37	11.68301868	0.00298712	0.059716996
XLOC_003526	391	651	6611	6638	28	11.57276775	0.003178953	0.059716996

Anril	1261	1651	214	253	40	11.52450115	0.003206358	0.059716996
XLOC_004803	841	1121	6796	6824	29	11.4671199	0.003343382	0.059716996
XIST	16121	16501	5754	5792	39	11.44374046	0.003425596	0.059716996
XLOC_008174	1471	1671	7897	7917	21	11.43951251	0.003425596	0.059716996
MALAT1	7801	8231	2381	2424	44	11.3613475	0.00356262	0.059716996
ANCR	201	481	21	49	29	11.34906164	0.00356262	0.059716996
NEAT1	2371	2651	2884	2912	29	11.3422696	0.003590025	0.059716996
XLOC_008174	171	361	7767	7786	20	11.19859052	0.003891477	0.063190176
XLOC_012599	1721	2011	9374	9403	30	11.02510137	0.004220334	0.065821488
lincMKLN1_A1	2431	2871	9757	9801	45	11.00709705	0.004247739	0.065821488
FIRRE(MM)	4501	4691	1497	1516	20	10.96566859	0.004412168	0.065821488
FIRRE(HG)	21	351	755	788	34	10.95680657	0.004439572	0.065821488
XIST	12761	13101	5418	5452	35	10.76196645	0.005015073	0.069526994
XIST	6921	7171	4834	4859	26	10.69724963	0.005097287	0.069526994
XLOC_009233	231	591	8063	8099	37	10.68621286	0.005097287	0.069526994
MALAT1	6851	7241	2286	2325	40	10.67982146	0.005097287	0.069526994
XLOC_004803	1371	1651	6849	6877	29	10.36394416	0.006001644	0.079235291
XLOC_009702	721	901	8181	8199	19	10.26805505	0.006467525	0.079235291
XLOC_010017	331	571	8333	8357	25	10.24913754	0.006467525	0.079235291
XIST	6051	6211	4747	4763	17	10.2314455	0.006522335	0.079235291
XLOC_002746	2311	2631	6474	6506	33	10.18266181	0.006604549	0.079235291
NEAT1	491	621	2696	2709	14	10.15253406	0.006741573	0.079235291
MALAT1	7431	7581	2344	2359	16	10.07693976	0.007015621	0.079235291
XLOC_008174	541	701	7804	7820	17	10.01526494	0.007289668	0.079235291
XLOC_010017	1531	1781	8453	8478	26	9.98929264	0.007426692	0.079235291
lincSFPQ	1841	2141	9994	10024	31	9.942391236	0.007508907	0.079235291
XIST	2971	3171	4439	4459	21	9.877254967	0.007755549	0.079235291
TUG1	1781	2101	3608	3640	33	9.867881366	0.007782954	0.079235291
lincMKLN1_A1	891	1131	9603	9627	25	9.831878803	0.007919978	0.079235291
NEAT1	331	451	2680	2692	13	9.81284518	0.008057002	0.079235291
BORG	1111	1431	368	400	33	9.782576326	0.008194026	0.079235291
MALAT1	2521	2901	1853	1891	39	9.77752032	0.008221431	0.079235291
TUG1	1361	1681	3566	3598	33	9.767173639	0.008221431	0.079235291
XLOC_006922	1631	1841	7720	7741	22	9.763916247	0.008221431	0.079235291
NR_024412	681	961	3090	3118	29	9.749488125	0.008221431	0.079235291
XIST	381	621	4180	4204	25	9.740872842	0.008248835	0.079235291
lincMKLN1_A1	71	361	9521	9550	30	9.718595048	0.008248835	0.079235291
XLOC_006922	191	301	7576	7587	12	9.61563693	0.008659907	0.082028562

GAS5	191	581	1555	1594	40	9.556464433	0.008988764	0.083012959
XLOC_005764	2481	2681	7510	7530	21	9.541211311	0.009098383	0.083012959
lincMKLN1_A1	1561	1851	9670	9699	30	9.508742545	0.009262812	0.083012959
XLOC_005151	1741	1931	7130	7149	20	9.499559434	0.009317621	0.083012959
NR_024412	1	321	3022	3054	33	9.487733444	0.009372431	0.083012959
lincSFPQ	1391	1531	9949	9963	15	9.402578042	0.009920526	0.086741011
TUG1	5531	5911	3983	4021	39	9.388324727	0.010084955	0.087062521
TUG1	2381	2491	3668	3679	12	9.335727122	0.010386407	0.087450984
XLOC_008174	2351	2661	7985	8016	32	9.335169811	0.010386407	0.087450984
Meg3	1091	1191	2582	2592	11	9.278524991	0.01063305	0.088435856
Anril	81	231	96	111	16	9.228506729	0.010907098	0.089622177
XLOC_008174	751	821	7825	7832	8	9.159841288	0.01126336	0.090227838
NR_029435	2051	2331	3341	3369	29	9.134362622	0.011345574	0.090227838
XIST	9151	9431	5057	5085	29	9.117188944	0.011482598	0.090227838
XIST	9811	9921	5123	5134	12	9.113299648	0.011510003	0.090227838
MALAT1	3961	4401	1997	2041	45	9.076917904	0.011756646	0.091114004
NEAT1	2861	3121	2933	2959	27	9.046833402	0.011948479	0.091396408
XLOC_011185	891	1091	8807	8827	21	9.023369996	0.012167717	0.091396408
lincMKLN1_A1	521	651	9566	9579	14	9.020322347	0.012195122	0.091396408
XIST	4491	4631	4591	4605	15	8.826916519	0.013400932	0.095955113
XIST	16641	16871	5806	5829	24	8.817645092	0.013537956	0.095955113
lincMKLN1_A1	671	811	9581	9595	15	8.81763317	0.013537956	0.095955113
XLOC_010017	1111	1311	8411	8431	21	8.815631478	0.01356536	0.095955113
XLOC_008174	441	521	7794	7802	9	8.804086668	0.01356536	0.095955113
GAS5	21	171	1538	1553	16	8.78673623	0.013647575	0.095955113
Meg3	1341	1471	2607	2620	14	8.749308529	0.013866813	0.096093298
MALAT1	971	1171	1698	1718	21	8.733773256	0.013949027	0.096093298
XIST	15351	15591	5677	5701	25	8.680936005	0.014223075	0.096565269
FIRRE(MM)	3011	3381	1348	1385	38	8.665956832	0.014332694	0.096565269
MALAT1	7611	7751	2362	2376	15	8.648774192	0.014469718	0.096565269
Meg3	731	871	2546	2560	15	8.62001438	0.014688956	0.096565269
NR_029435	601	841	3196	3220	25	8.577164138	0.015045218	0.096565269
XLOC_002746	2101	2251	6453	6468	16	8.565846696	0.015127432	0.096565269
NR_029435	111	241	3147	3160	14	8.539550461	0.015209646	0.096565269
XLOC_010514	631	791	8585	8601	17	8.532789269	0.015209646	0.096565269
XLOC_002408	631	951	6199	6231	33	8.518004657	0.015291861	0.096565269
XLOC_002746	521	791	6295	6322	28	8.473451979	0.015620718	0.09773697

744